

Organic Thin-Film Transistors with Inkjet-Printed Electrodes on Hydrophobic Teflon-AF Gate Dielectric with Reversible Surface Properties

Paria Naderi and Gerd Grau*

Department of Electrical Engineering and Computer Science, York University, Toronto, Canada

* panaderi@yorku.ca

Keywords: Organic thin-film transistors (OTFT), Hydrophobic gate dielectric, Teflon-AF amorphous fluoropolymer, Semiconductor/dielectric interface, Printed electronics, Inkjet-printed electrodes

Abstract

Printed organic thin-film transistors (OTFTs) are promising for flexible, low-cost electronics; however, a major challenge is that successive processing steps of multiple solution-processed layers can interfere with each other. In particular, hydrophobic fluoropolymers are a promising group of materials to fabricate gate dielectrics with low charge trap density and properties such as good thermal stability, chemical inertness, low dielectric constant, and water repellency. However, the main difficulty in incorporating hydrophobic fluoropolymers in printed electronic devices is their low surface energy. Plasma treatment is a common method for surface modification that renders these hydrophobic layers wettable to print subsequent layers. This plasma processing can

also affect the interface with the organic semiconductor (OSC) and transistor performance, which is studied here for the first time. The morphological and surface chemical properties of Teflon amorphous fluoropolymer (Teflon-AF) films change after plasma treatment and gradually reverse after post-annealing of subsequent layers as demonstrated here. Here, we fabricate solution-processed OTFTs with Teflon-AF as the gate dielectric. We report OTFTs with inkjet-printed source and drain electrodes with a minimum channel length of 20 μm on Teflon-AF for the first time. We show that the annealing of the inkjet-printed electrodes changes the morphology and the surface chemistry of the Teflon-AF gate dielectric underneath, thus reversing the effect of the plasma. We show that this electrode post-annealing step can improve the transistor performance by improving the interface between the Teflon-AF gate dielectric and the OSC in terms of smoothness and hydrophobicity. The transistor parameters such as mobility, on/off current ratio, and threshold voltage all follow a trend explained here by the properties of the Teflon-AF films. Increasing the post-annealing temperature to just below complete surface reversibility decreases surface roughness and trap-sites created after plasma treatment leading to optimized device performance. We characterize the Teflon-AF surface with contact angle measurement, roughness measurement, Fourier transform infrared spectroscopy (FTIR), and x-ray photoelectron spectroscopy (XPS). This understanding of the reversibility of the Teflon-AF surface helps achieve optimal performance of devices and systems incorporating fluoropolymers.

1. Introduction

Printed organic electronics offers many potential advantages, including low-cost and low-temperature manufacturing, chemical tailorability of materials, mechanical flexibility, and large-area printability [1]. OTFTs are the fundamental components of many circuits, and improving their performance is a key to improving printed electronics [2–4]. OTFTs have four layers: the gate

electrode, the gate dielectric, the source and drain electrodes, and the organic semiconductor (OSC). Since charge transport happens within a few nanometers from the OSC/ dielectric interface, the dielectric surface properties become very important [5–7]. Using fluoropolymers as the gate dielectric has a number of advantages. Due to their water-repellency, fluoropolymers are used in transistors as the gate dielectric or encapsulation to prevent possible doping and charge trapping in the channel [8,9]. A smoother dielectric surface leads to larger grain sizes and fewer defects in the OSC channel [10,11]. Other than their water-repellency and smooth surfaces, fluoropolymers have low dielectric constant, which enhances the charge transport in the semiconductor channel [12]. The strong C-C and C-F bonds are what make fluoropolymers unique. Their interesting properties such as thermal stability, chemical inertness, and low dielectric constant have made them suitable candidates for tubing and coating, cable insulation, cardiovascular grafts, and protective coating in printed circuit boards [13–15]. For instance, Teflon-AF has been used as the gate dielectric in solution-processed organic thin-film transistors (OTFTs) [9,16–19] because of its interesting properties such as low refractive index (~ 1.3), low dielectric constant (~ 1.9), and high optical transparency (from around 200 nm to 2000 nm wavelength).

Despite their desirable properties, it can be quite challenging to incorporate hydrophobic fluoropolymers in solution-processed electronic devices. Due to their low surface energy, one can not easily form patterns on these films through low-viscosity solution-processing techniques such as inkjet printing of OTFT electrodes. To combat this wettability issue, surface modification is often performed on these films to decrease their hydrophobicity. Plasma treatment is a common method for surface modification. It is convenient, it changes the surface without tampering with the bulk, its effect is uniform, and it does not require the use of hazardous chemicals [20]. Some studies have investigated the nature of surface modification of fluoropolymers such as crystalline

PTFE through plasma treatment [20–24]. Plasma-etching on evaporated and spin-coated Teflon-AF films increases the film's roughness and alters its chemical bonds on the surface [25]. These studies show that the morphology and the surface chemistry of the material are modified after plasma treatment.

In many reports, OTFTs with hydrophobic gate dielectric are limited to vacuum processed electrodes due to the difficulty of printing electrodes and/or the OSC onto a hydrophobic dielectric [26,27]. There are examples of solution-processed electrodes in OTFTs with conductive inks such as silver and gold on surface-modified hydrophobic gate dielectrics like Teflon-AF and Cytop. To overcome the low surface energy of fluoropolymers, some reports used selective surface energy patterning combined with blanket coating of metal nanoparticle inks, which requires a mask and is difficult on heterogeneous substrates [18,28]. Another method is dispenser printing combined with plasma surface modification, however, the resolution is low [17]. Therefore, there is a need to study scalable, high-resolution printing methods such as inkjet printing to fabricate OTFT electrodes on fluoropolymers. Furthermore, the effect of surface-modification on these fluoropolymer surfaces and the OSC/dielectric interface has not been studied so far.

In other contexts, some reports show that heat recovers the surface of different fluoropolymers after they have been modified either by plasma treatment or humidity. Ridges and rough spots formed on Cytop after long hours of submersion in water disappear after heat treatment and the smoothness of the surface is recovered [29]. Also, annealing of water-immersed fluorinated amorphous carbon (a-C:F) coatings eliminates the effects produced by humidity and decreases degradation due to water exposure [30]. This property has been used to restore the hydrophobicity of a Teflon-AF mold in order to form a semiconductor layer only between certain islands on the surface [31].

In a solution-processed bottom-gate-bottom-contact (BGBC) OTFT, the hydrophobic gate dielectric undergoes a series of processing steps. After the dielectric film is solution-deposited, it is annealed once for its solvent to evaporate. Then, the film surface is modified to increase its wettability to prevent dewetting and improve adhesion of the next solution-processed layer. Finally, with the annealing of the next layer (electrodes or another polymer layer), the gate dielectric is also annealed at least one more time. When using fluoropolymers as the gate dielectric, this post-annealing step can reverse the effect of the plasma treatment.

In this paper, we report OTFTs with inkjet-printed silver source and drain electrodes on a fluoropolymer gate dielectric with a minimum channel length of 20 μm , which has not been reported before. We obtained these high-resolution electrodes without the use of masks or subtractive processes. We study the effect of the electrode processing on Teflon-AF as the gate dielectric and take advantage of its reversible properties to engineer the OSC/dielectric interface. Teflon-AF is plasma treated to facilitate printing of the electrodes. Afterwards, it is post-annealed when the inkjet-printed electrodes are being annealed, which also reverses the effect of the plasma. In fact, plasma treatment is usually performed on hydrophobic dielectrics before the solution deposition of the OSC [32,33]. However, here we show that a direct deposition of the OSC on a plasma treated Teflon-AF results in very low performance. Therefore, a dielectric post-annealing step is necessary to restore the surface both morphologically and chemically. In other words, this post-annealing step is a handle to control the OTFT performance. By varying the post-annealing temperature, the surface properties of Teflon-AF change, which causes the OSC/dielectric interface to change. We find that the state of the Teflon-AF surface clearly affects extracted transistor parameters such as mobility, on-current, off-current, on/off current ratio, and the threshold voltage. To distinguish between contact resistance effects and OSC/ dielectric interface

effects, we extract the contact resistance and low-field mobility of the devices. After ascribing the changes in OTFT performance to the OSC/ dielectric interface, we study the Teflon-AF films with different characterization techniques: contact angle measurement, roughness measurement, Fourier transform infrared spectroscopy (FTIR), and x-ray photoelectron spectroscopy (XPS). Our findings show that after plasma treatment, the wettability, roughness, and the percentage of reactive elements like oxygen increase on the surface of the films. However, they all decrease after post-annealing corresponding to improvements in the OTFT performance. This confirms the importance of Teflon-AF surface reversibility to engineer the OSC/ dielectric interface in a printed transistor fabrication process.

2. Materials and methods

OTFT fabrication: The transistors were fabricated on indium tin oxide (ITO)-coated glass slides (Sigma-Aldrich, Oakville, Canada). The ITO film was used as the gate electrode. Teflon-AF 1600 (Sigma-Aldrich, Oakville, Canada) was dissolved in Fluorinert FC-40 (Sigma-Aldrich, Oakville, Canada) in a 1.6 wt. % solution. The solution was spin-coated in two steps at 600 rpm for 1 minute and dried at 150 °C for 15 minutes each time, resulting in an overall thickness of 450 nm. The capacitance per unit area and the dielectric constant are 3.53 nF/cm² and 1.83 respectively (details in the Supplementary Information). The Teflon layer was then air plasma-treated for 1 minute at 200 W with a PE-50 plasma system (50kHz). The source and drain electrodes were inkjet-printed using a silver nanoparticle ink (ANP DGP 40LT-15C, Advanced Nano Products, Co., Sejong, Korea). A custom-built inkjet printer with a 60 µm diameter nozzle (MJ-ATP-01-60-8MX, Microfab Technologies, Inc. Plano, TX) was used. The channel width of the devices was 1,300 µm, and the channel length was varied from 20 µm to 75 µm. The printed source and drain electrodes were dried first at 60 °C for 5 minutes to prevent the coffee ring effect and then annealed

at different temperatures for the purpose of this study. The organic semiconductor poly(2,5-bis(2-octyldodecyl)-3,6-di(pyridin-2-yl)-pyrrolo[3,4-c]pyrrole-1,4(2H,5H)-dione-alt-2,2'-bithiophene) (PDBPyBT) (Ossila Ltd, Sheffield, UK) was dissolved in chloroform with 10 mg/ml concentration and was spin-coated at 3,000 rpm followed by annealing at 120 °C for 10 minutes. To study the effect of plasma treatment directly on the OTFT performance, devices with no post-annealing condition were also tested. In this case, after annealing printed electrodes at two different temperatures (100 °C and 160 °C), the samples were plasma treated one more time. Samples for Teflon-AF characterization were fabricated in the same way without the printed electrodes and the organic semiconductor.

The devices were fabricated and tested in ambient conditions. The transistor I-V characteristics were obtained using a semiconductor parameter analyzer (Keithley 4200, Tektronix).

Contact angle measurements: The contact angle of deionized (DI) water was measured using a Kruss DSA10 contact angle measurement system. Each error bar was calculated using 12-14 data points.

Roughness measurements using atomic force microscopy (AFM): The roughness of the Teflon-AF films and the thickness and roughness of the OSC layers were measured with a Multimode 8 scanning probe microscope (SPM). The imaging mode was ScanAssist-air. Each error bar was calculated using 12-18 data points obtained from different samples and different spots on the same sample.

FTIR measurements: For attenuated total reflection (ATR) measurements, a Vertex 70v FTIR spectrometer was used. The measurements were carried out in absorption mode.

XPS measurements: The survey spectra were obtained from a K-Alpha XPS spectrometer. They were also repeated with ESCALAN 250Xi. The energy scale was adjusted to place the carbon main peak (C-C) at 285 eV.

3. Results and discussion

3.1 OTFT performance: parameters and contact resistance

The complete OTFT fabrication process is shown in a. In the BGBC configuration employed here, the dielectric layer is followed by the inkjet-printed silver nanoparticle source and drain electrodes. However, if the Teflon-AF surface is left untreated, the ink does not spread sufficiently, and the droplets do not connect to form lines. Instead, the ink dewets the Teflon-AF surface, and the droplets bulge up. For this reason, the Teflon-AF layer is air plasma-treated. Figure 1b and c show the printed source and drain electrodes without and with plasma treatment. The final device with a channel length of 20 μm with the OSC spin-coated on top is shown in Figure 1d.

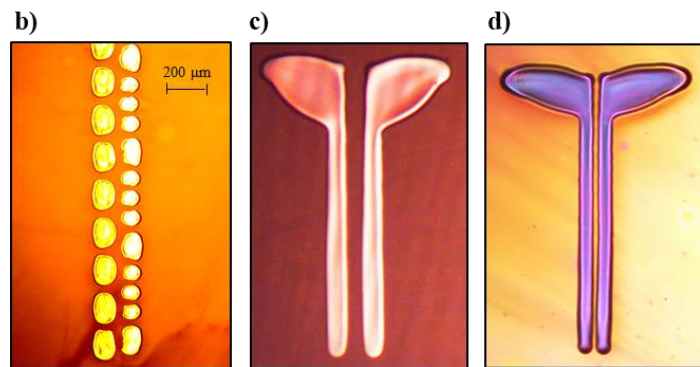
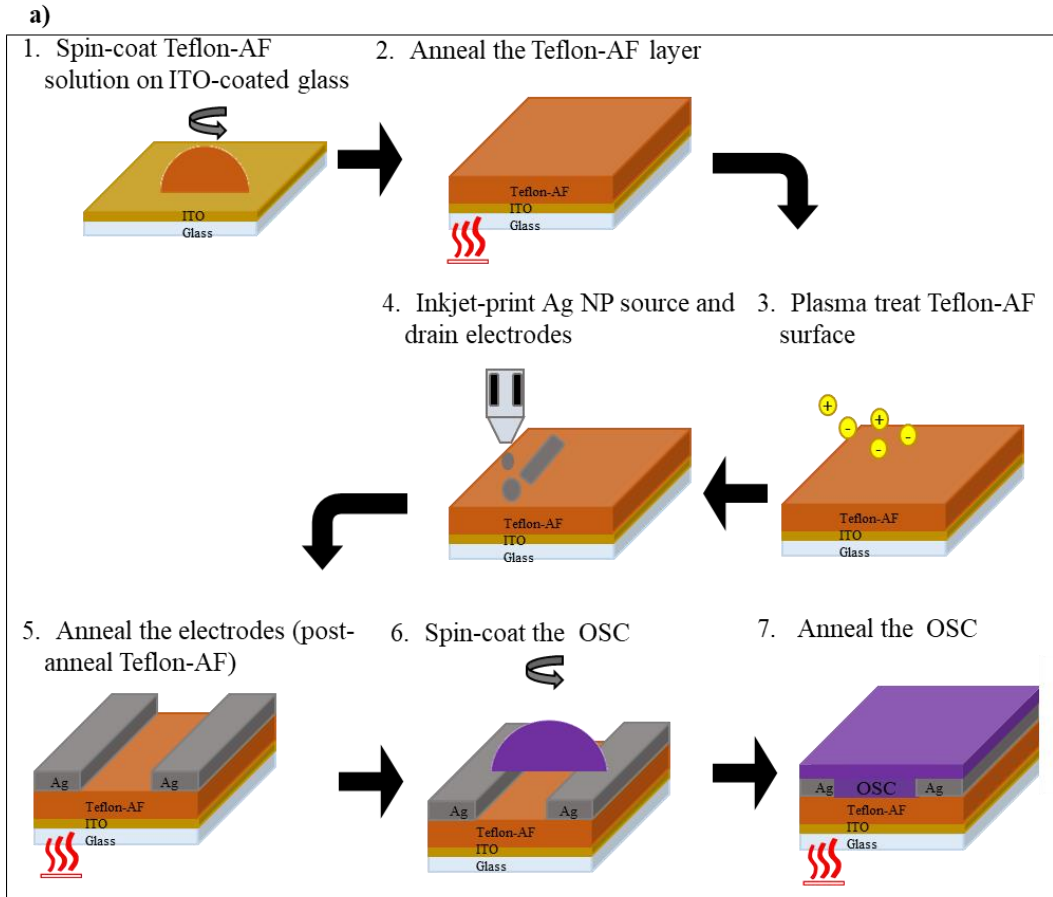


Figure 1. (a) OTFT fabrication process. Optical micrographs of printed source and drain electrodes (b) without plasma treatment, (c) with plasma treatment, and (d) the final device with 20 μm channel length and the OSC spin-coated on top.

Figure 2a shows the output characteristics ($I_d V_d$) of a 20 μm channel length device with electrodes post-annealed at 160 $^\circ\text{C}$, and Figure 2b shows the transfer characteristics ($I_d V_g$) at $V_d = -120\text{ V}$ of 20 μm channel length devices without and with different post-annealing temperatures. As can be seen from Figure 2b, the on-current values and the slope of the square root of the drain current are higher for post-annealing temperatures of 120 $^\circ\text{C}$, 140 $^\circ\text{C}$, and 160 $^\circ\text{C}$. The devices below and above this range show clear deterioration in performance. Figure 3 shows the performance trend versus the post-annealing temperature for average and maximum saturation field-effect mobility (μ_{sat}), average and maximum linear field-effect mobility (μ_{lin}), average and maximum on-current (I_{on}) normalized by channel width and length, log of off-current ($\text{Log}(I_{off})$), threshold voltage (V_{th}), saturation subthreshold swing (SS), and log of on-off current ratio ($\text{Log}(\frac{I_{on}}{I_{off}})$) These parameters were averaged over the whole range of channel lengths from 20 μm to 75 μm . The saturation field-effect mobility is calculated from the slope of the square root of the drain current versus gate voltage from $I_d V_g$ characteristics in the saturation regime:

$$\mu_{sat} = \frac{2L}{C_{ox}W} \left(\frac{\partial \sqrt{I_d}}{\partial V_g} \right)^2 \quad (1)$$

where W and L are the channel width and length of the transistor channel, and C_{ox} is the dielectric capacitance per unit area. Devices with no post-annealing have low performance. The devices post-annealed at 160 $^\circ\text{C}$ have the highest mobility (average: 0.12 $\text{cm}^2/\text{V.s}$ and maximum: 0.19 $\text{cm}^2/\text{V.s}$), and the devices post-annealed at 120 $^\circ\text{C}$ have the highest on/off current ratio (average: 5.5×10^5 and maximum: 3.4×10^6). The saturation field effect mobility and the on-current are highest at post-annealing temperatures between 120 $^\circ\text{C}$ and 160 $^\circ\text{C}$. The other parameters are initially constant with post-annealing temperature up to 160 $^\circ\text{C}$. At this point, V_{th}

abruptly starts becoming more negative, SS and I_{off} increase and I_{on}/I_{off} decreases. Two different regimes can be observed. At low post-annealing temperatures, on-state performance increases as the post-annealing modifies the Teflon-AF dielectric. At high post-annealing temperatures, both on- and off-state performance deteriorate. Therefore, it is important to identify the optimal post-annealing temperature. It is worth noting that other transistors fabricated using this OSC (PDBPyBT) or other DPP derivatives, have used evaporated source and drain contacts and inert atmosphere processing conditions for the OSC [27,34,35]. The transistors fabricated here, despite having inkjet-printed contacts and ambient atmosphere processing for the OSC, show comparable performance to transistors with the same device structure and otherwise same OSC processing conditions.

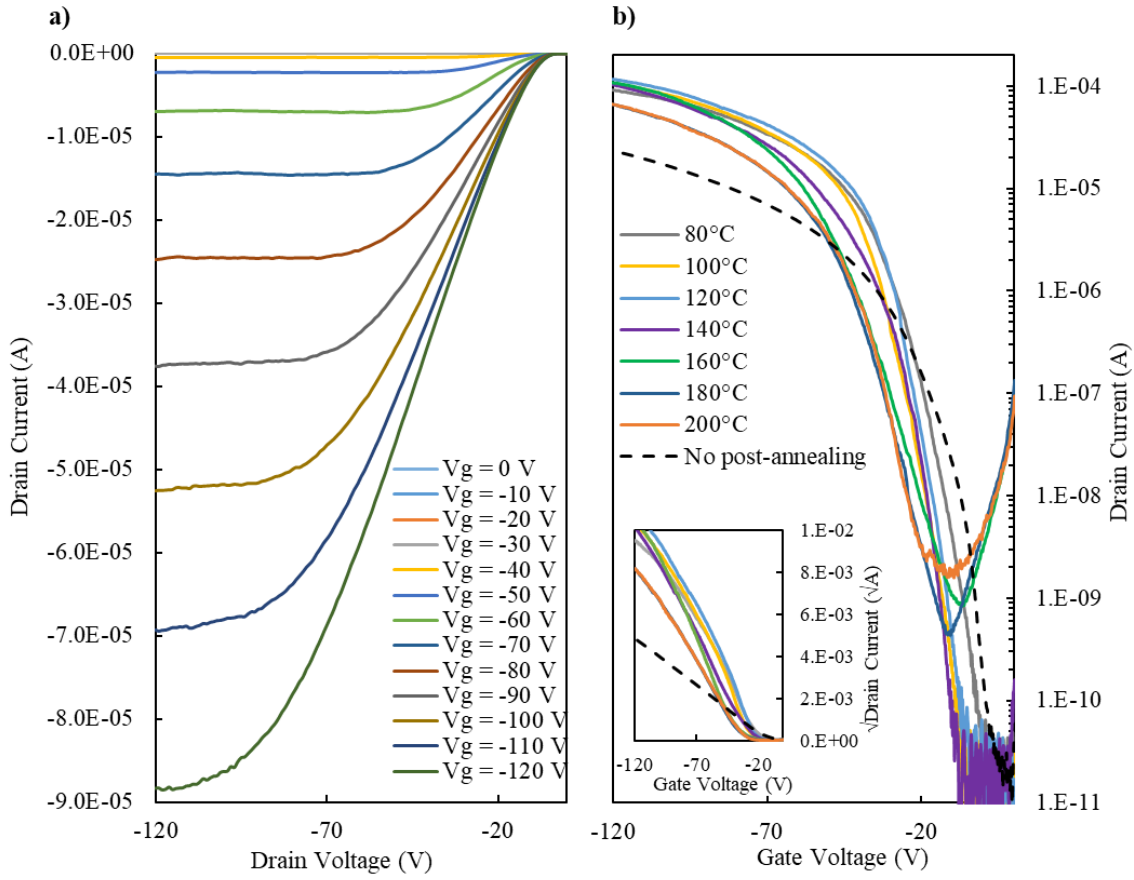


Figure 2. (a) Output characteristics ($I_d V_d$) of a $20\ \mu\text{m}$ channel length device post-annealed at 160°C and (b) transfer characteristics ($I_d V_g$) at $V_d = -120$ V of $20\ \mu\text{m}$ channel length devices without and with different post-annealing temperatures. Inset shows the square root of drain current versus post-annealing temperature.

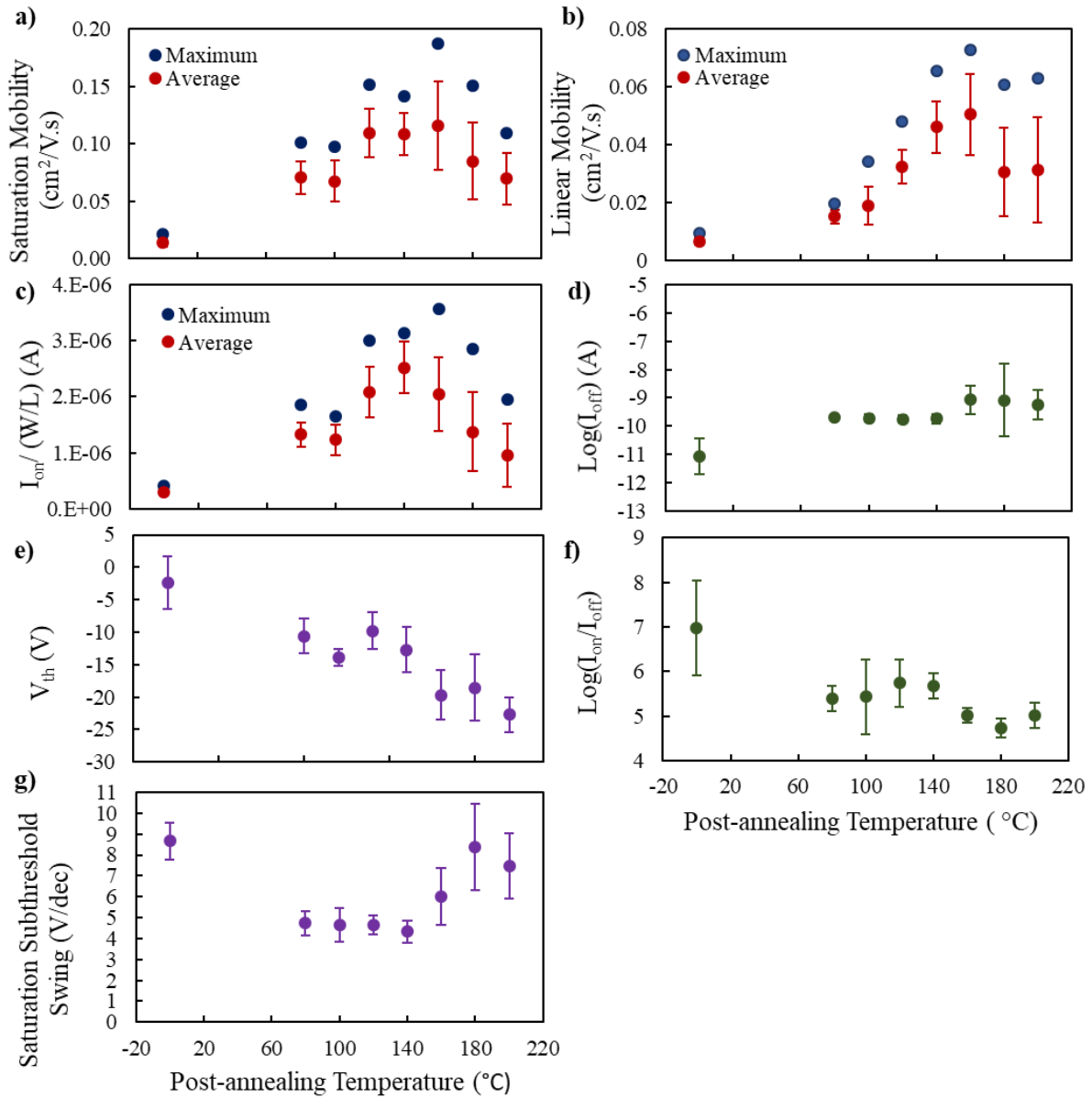


Figure 3. Graphs of (a) average and maximum saturation field-effect mobility extracted at $V_d = -120$ V, (b) average and maximum linear field-effect mobility extracted at $V_d = -20$ V, (c) Average and maximum width and length normalized on-current, (d) log of off-current, (e) threshold voltage, (f) log of on-off current ratio, and (g) saturation subthreshold swing.

As shown in Figure 3 , a clear trend is observed between all OTFT parameters and Teflon-AF post-annealing temperature with different regimes. There are different phenomena affecting the performance of organic transistors. For instance, controlling the OSC/ dielectric interface with the aim of minimizing the trap density in the channel can lead to high mobility devices [36,37]. At the same time, it is well-known that organic field-effect transistors suffer from limitations caused by contact resistance [38], and since the post-annealing temperature is, in fact, the silver annealing temperature, it may affect the contact resistance. To understand the effect of contact resistance, two methods were used, the transmission line method (TLM) and, the Y-function method (YFM). For TLM, the total resistance was extracted from the inverse of the slope of the output characteristics in the linear regime. Then, it was plotted versus channel length varying between 20 – 75 μm . The width normalized contact resistance and channel resistance per channel length were extracted from the y-intercept and the slope of the plots. The result is shown in Figure 4a and b.

Concurrently, the low-field mobility and the contact resistance were extracted with YFM. Low-field mobility is the intrinsic carrier mobility of the transistor, which is not affected by contact resistance. The YFM technique is introduced in detail in Ref. [38]. In the YFM, the transfer characteristic ($I_d V_g$) in the linear regime is used. Using the current equation in the linear regime, the Y function is defined as:

$$Y = \frac{I_d}{\sqrt{g_m}} = \sqrt{\frac{W}{L} C_{ox} \mu_0 V_d} \times (V_g - V_t) \quad (2)$$

where g_m is the transconductance, W and L are the channel width and length of the transistor, C_{ox} is the dielectric capacitance per unit area, μ_0 is the low-field mobility, V_d is the drain current (here -20 V), and V_t is the threshold voltage. From the slope of Y versus V_g , μ_0 is obtained and

from the x-intercept, V_t is extracted. To calculate contact resistance, mobility attenuation factor θ was extracted, which gives us contact resistance:

$$\theta = \theta_0 + \theta^* = \theta_0 + G_m \times R_{sd} \quad (3)$$

where θ_0 (≈ 0), G_m and R_{sd} are the mobility reduction coefficient, transconductance parameter, and the source-drain contact resistance, respectively. In the next step, we plot $\frac{1}{\sqrt{g_m}}$ versus $V_g - V_t$, using the below equation:

$$\frac{1}{\sqrt{g_m}} = \frac{1 + \theta(V_g - V_t)}{\sqrt{\frac{W}{L} C_{ox} \mu_0 V_d}} \quad (4)$$

From the x-intercept, we extracted θ , from which we can obtain contact resistance. The low-field mobility and the contact resistance ($R_c = R_{sd}/2$) for all the post-annealing temperatures calculated using the YFM are shown in Figure 4c and d. The low-field mobility changes with post-annealing temperature with the maximum value at 160 °C (Figure 4d) and it exhibits the same trend as the saturation field-effect mobility shown in Figure 3a. The contact resistance values extracted from the two methods (Figure 4a and c) are very close to each other and follow the same trend, which confirms the reliability of both methods in proving that the contact resistance is independent of post-annealing temperature. Furthermore, the trends seen in channel resistance and low-field mobility are in the same direction (Figure 4b and d).

Therefore, here with contact resistance not changing and μ_0 and channel resistance changing with post-annealing temperature, we conclude that the main factor contributing to the change in transistor performance is the change in the OSC/dielectric interface. Hence, in the following sections, the effect of the post-annealing on the Teflon-AF surface wettability, morphology, and chemistry are studied. It is worth noting that the devices with no post-annealing had two different

silver annealing temperatures (100 °C and 160 °C) and performed very similarly to each other (details in the Supplementary Information).

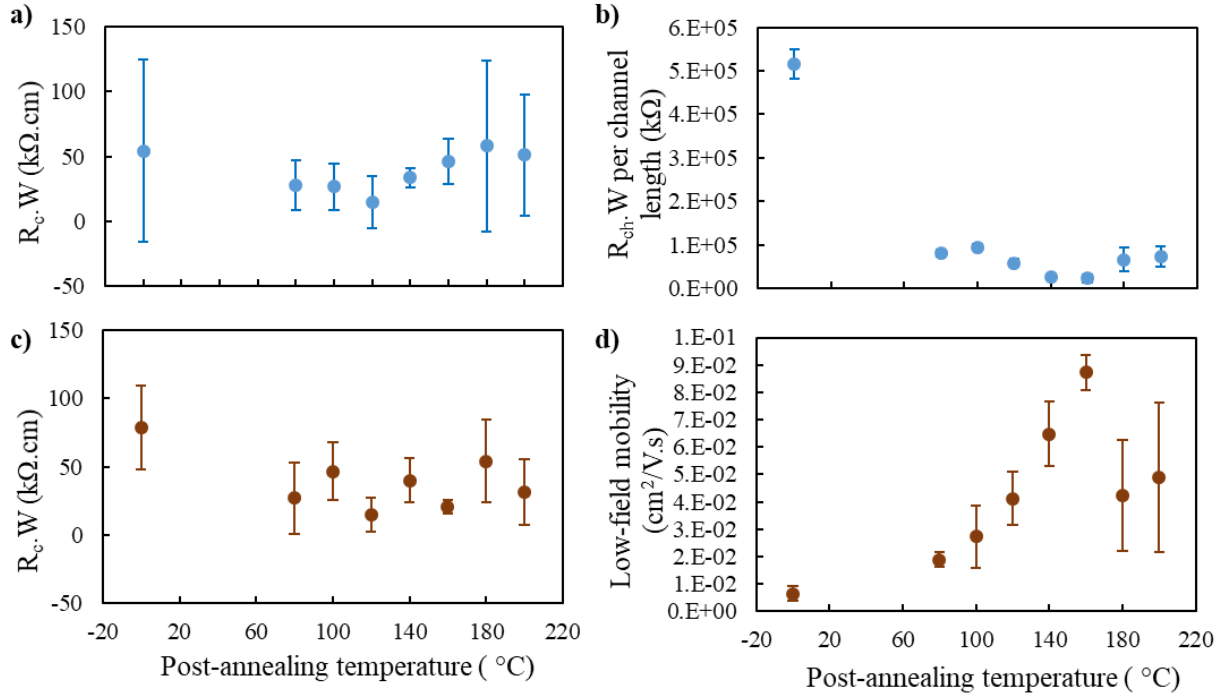


Figure 4. Width normalized (a) contact resistance, and (b) channel resistance per channel length calculated using TLM. (c) Width normalized contact resistance, and (d) low-field mobility calculated using YFM. The contact resistance values extracted from the two methods are very close to each other and show that the contact resistance is independent of post-annealing temperature.

3.2 Wettability: water contact angle measurements on Teflon-AF films

The advancing and receding contact angles (CA), along with the contact angle hysteresis of DI water droplets on Teflon-AF films before and after air plasma treatment and after the post-annealing step, are presented in Figure 5a. The advancing CA before plasma treatment is 118.4°, which means the surface is hydrophobic. The receding contact angle is slightly lower and is equal

to 109.7°. Therefore, the contact angle hysteresis is just below 10°. After plasma treatment, the advancing and receding contact angles drop to 101.7° and 36° respectively (still considered as hydrophobic), causing the CA hysteresis to increase to 66°. After post-annealing the films at 80 °C, the advancing CA increases to 118.1°. For higher annealing temperature, it increases further at a slow rate up to 121° at 200 °C. Conversely, the receding CA is still low at 80 °C (66°) and has a higher rate of increase to 109.7° at 200 °C. Thus, the CA hysteresis decreases from 66° to 10.3°. The receding CA changes most dramatically following the plasma treatment and post-annealing steps. Figure 5b-e show the difference in the receding CA for 80 °C and 200 °C post-annealing temperatures, while their advancing CAs are not very different. The high CA hysteresis and overall lower CA at lower post-annealing temperature are indicative of two possible causes: a rougher surface caused by plasma treatment or/and the presence of reactive elements caused by plasma treatment which results in liquid sorption and wetting of the surface. Likewise, the low CA hysteresis and higher CA at higher post-annealing temperature can be explained by lower roughness or/and lower percentage of reactive elements, which prevent the wetting of the surface. Both roughness and surface chemistry of the dielectric/ OSC interface can affect transistor behavior. Additionally, changes in dielectric CA can affect the thickness of the solution-processed OSC and potentially OTFT performance. These different phenomena are investigated in the next

sections.

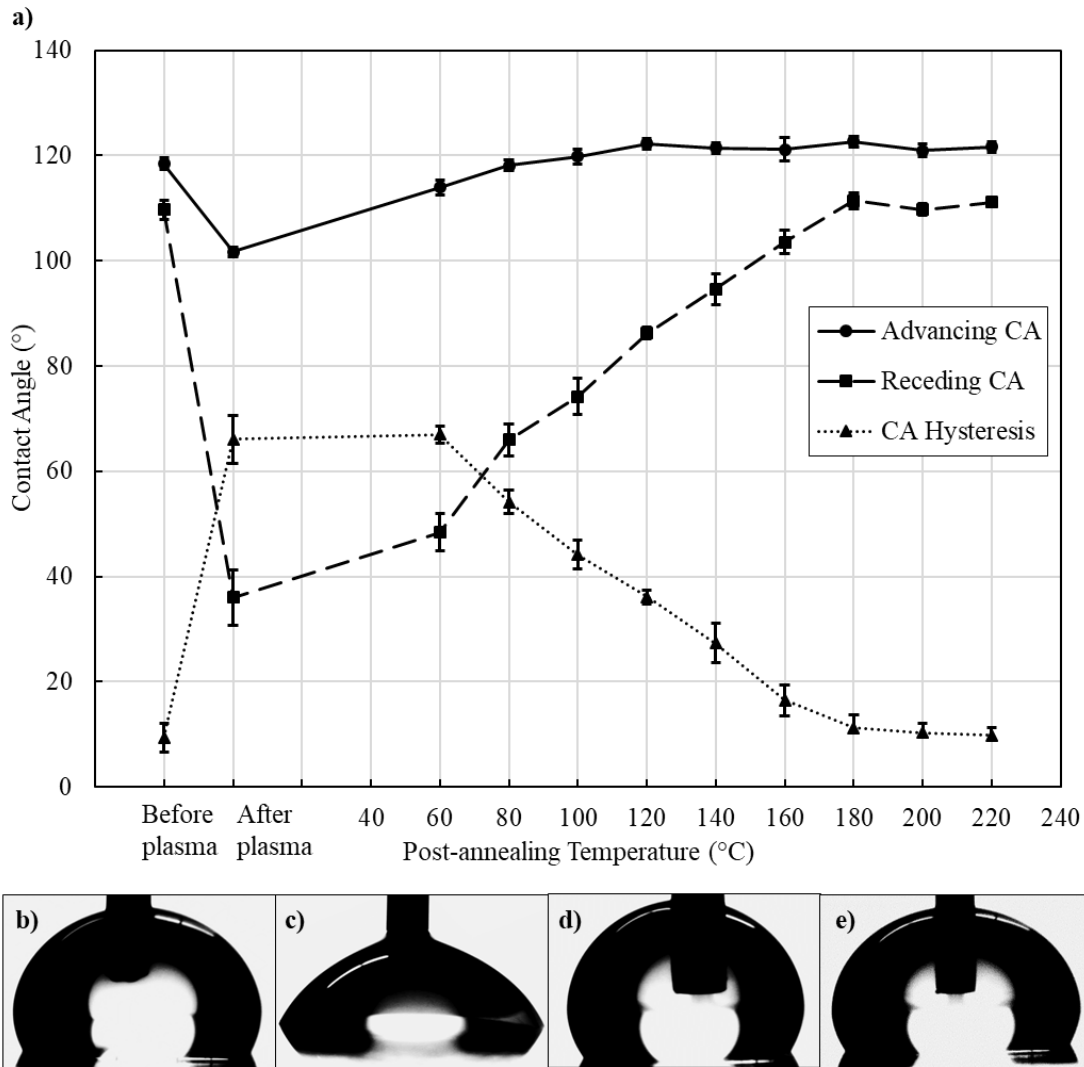


Figure 5. (a) Advancing and receding CA, and CA hysteresis of DI water on Teflon-AF films before and after air plasma treatment and after post-annealing. Both advancing and receding CA decrease after plasma treatment and recover with post-annealing. The decrease in receding CA is much larger than for advancing CA resulting in increased CA hysteresis after plasma treatment. Images of droplets on films post-annealed at 80 °C are shown in (b) for advancing and (c) receding mode. Similarly, droplets on films post-annealed at 200 °C are shown in (d) for advancing and (e) receding mode. The receding CA for samples post-annealed at 80 °C and 200 °C are very different, while the difference for advancing CA is smaller.

3.3 Organic semiconductor thickness

Figure 6 shows the OSC thickness versus Teflon-AF post-annealing temperature. At 180 °C and 200 °C, the OSC preferentially wets the source and drain electrodes and channel. It dewets from the Teflon-AF dielectric in other areas due to the low CA hysteresis. This increase in the OSC thickness can explain the increase in the transistor off-current (Figure 3d) beyond 160 °C. For lower Teflon-AF post-annealing temperatures, the OSC thickness varies less strongly but still increases with temperature due to the changing surface wettability. To confirm whether the changes in OTFT electrical characteristics with post-annealing temperature up to 160 °C are due to changes in the Teflon-AF surface properties or the OSC thickness, another set of devices was fabricated with a post-annealing temperature of 120 °C and a lower spin speed (2,000 rpm compared with 3,000 rpm for all other samples). The average OSC thickness expectedly increased from 114 nm to 182 nm, which is comparable to the 160 °C post-annealed devices with the best on-state performance. This thickness increase caused the off-current to increase from 1.8×10^{-10} A to 5.2×10^{-10} A. By decreasing the spin speed to 2,000 rpm, the interface-dependent parameter threshold voltage only changes marginally from -9.8 V to -9.3 V. The average saturation mobility and on-off current ratio decreased from 0.11 cm²/V.s to 0.08 cm²/V.s, and from 5.5×10^5 to 1.9×10^5 , respectively. Therefore, it can be concluded that OSC thickness cannot explain the improvement in OTFT performance with post-annealing.

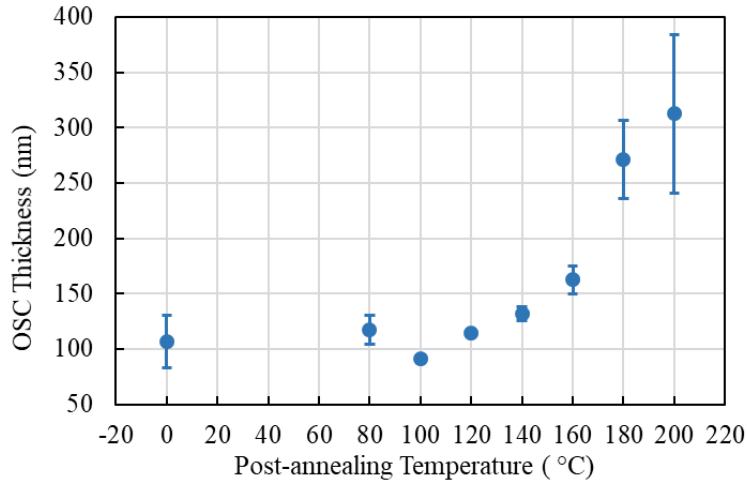


Figure 6. OSC thickness versus post-annealing temperature shows an increasing trend with increasing temperature.

3.4 Surface morphology: roughness measurement through atomic force microscopy (AFM)

Wettability is a factor that needs to be characterized alongside roughness [39]. Contact angle hysteresis is mainly the result of surface roughness. The roughness size can be in the micrometer [40] or nanometer range [41]. Experiments and simulations show that even atomic-scale roughness can lead to contact angle hysteresis [42]. Both peak-to-peak and average roughness (root mean square (RMS)) of the Teflon-AF films before and after plasma treatment and after post-annealing were measured and are presented in Figure 7. Both roughness measures increase after plasma treatment from 0.63 nm to 1.25 nm and from 4.61 nm to 8.28 nm for average and peak-to-peak roughness, respectively. They decrease after post-annealing at 80 °C to 1.1 nm and 7.97 nm for the average and peak-to-peak roughness, respectively. They continue to decrease slowly to 0.67 nm and 4.97 nm, respectively, at 200 °C. Both these roughness values help build a better understanding of how the surface morphology of the films changes through the plasma and post-

annealing steps. To have a complete understanding of the surface roughness, the AFM images representing each step are shown in Figure 8. Interestingly, after post-annealing the films, grain-like structures appear on the surface, and then by increasing the temperature, this grain-like structure disappears and the films become smooth again. The films start smoothing at 160 °C, which is the glass transition temperature (T_g) of the material. The decreasing surface roughness may explain the gradual increase in the on-current and saturation field-effect mobility with increasing post-annealing temperature (Figure 3a and c).

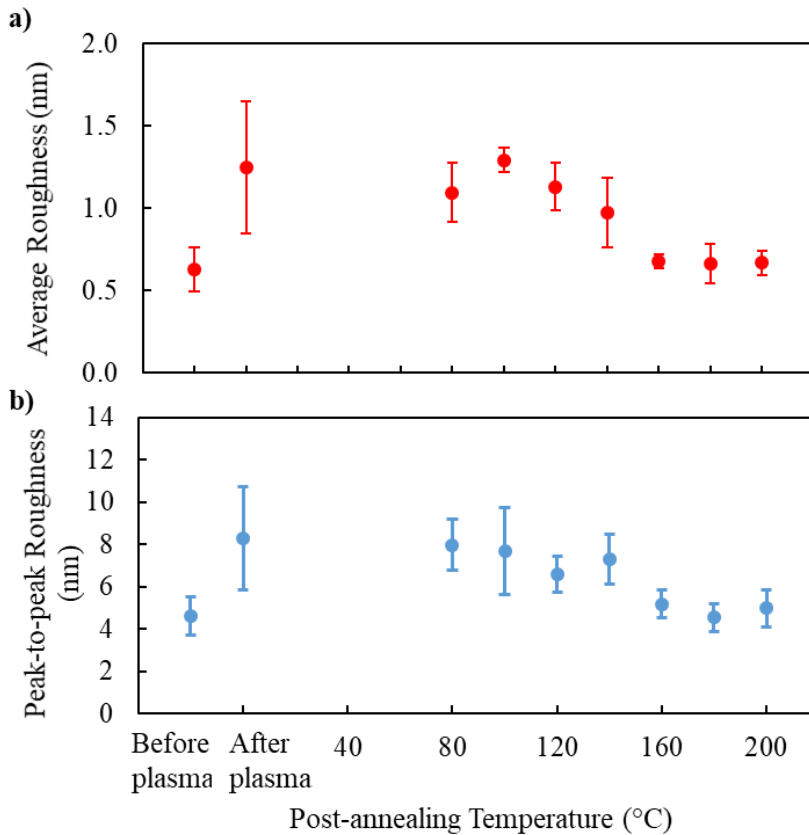


Figure 7. (a) Average and (b) peak-to-peak roughness of Teflon-AF films before and after plasma treatment and after post-annealing. Both roughness values increase after plasma treatment and decrease after post-annealing. At 200 °C, they approach their value before plasma treatment.

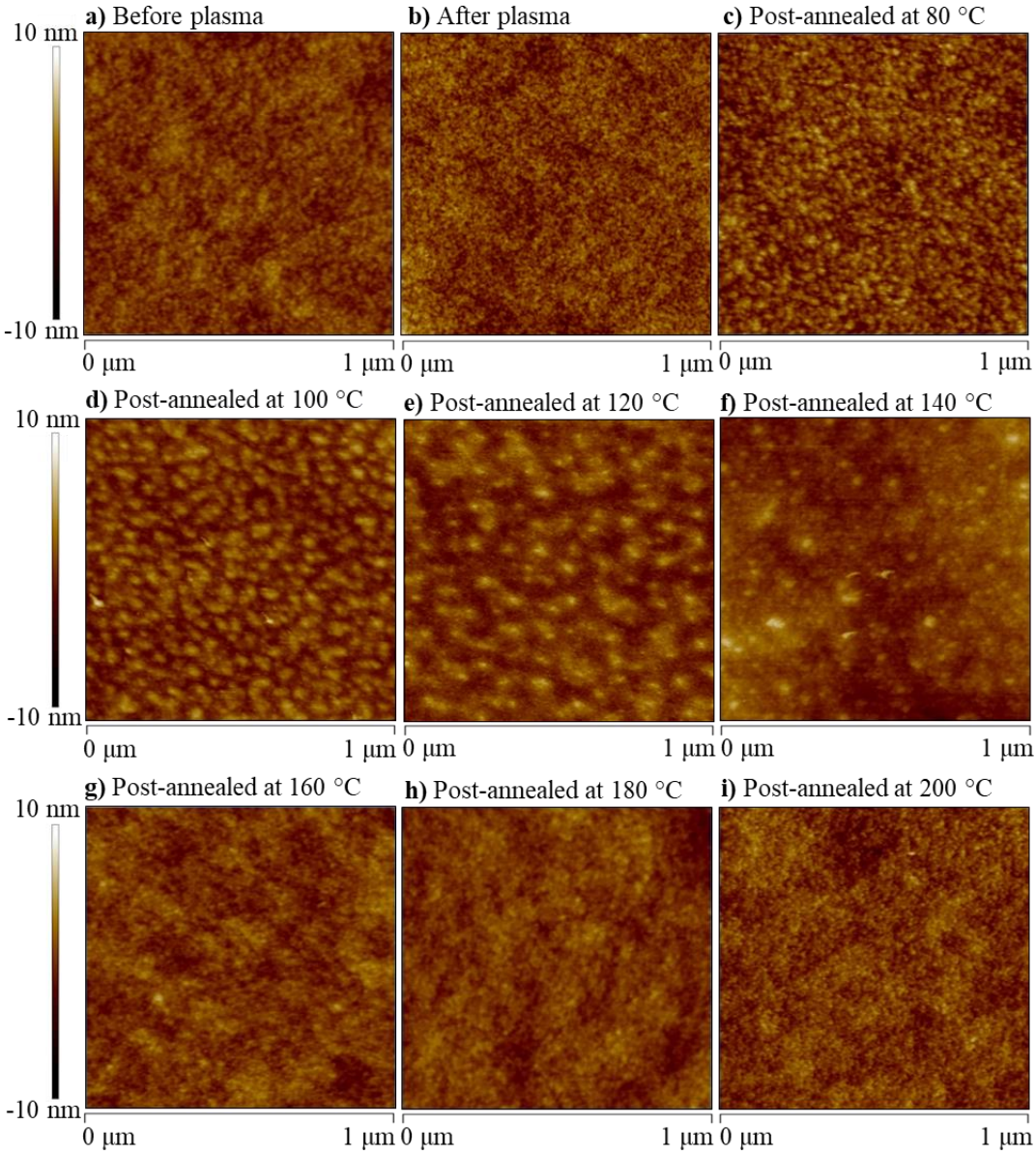


Figure 8. AFM images of the Teflon-AF films (a) before plasma, (b) after plasma, post-annealed at (c) 80 °C, (d) 100 °C, (e) 120 °C, (f) 140 °C, (g) 160 °C, (h) 180 °C, and (i) 200 °C.

It is well known that higher roughness causes a disordered structure in the OSC at the interface [43]. A smoother dielectric surface causes the formation of larger OSC grains at the interface, which leads to improved charge transport and field-effect mobility [44,45]. The average roughness data and AFM images of the OSC for different post-annealing temperature are shown in Figure 9

and Figure 10, respectively. The OSC roughness increases with increasing post-annealing temperature which indicates the increase of OSC grain size. The decrease in the CA hysteresis at high post-annealing temperatures with decreasing roughness matches well with theory. According to the Wenzel model, on hydrophobic surfaces, when the droplet is receding, larger roughness pins the contact line trying to stop the liquid from retracting, therefore, leading to a larger CA hysteresis [46–48]. However, the decrease in advancing contact angle after plasma cannot be understood in terms of surface roughness and the chemistry of the surface needs to be considered.

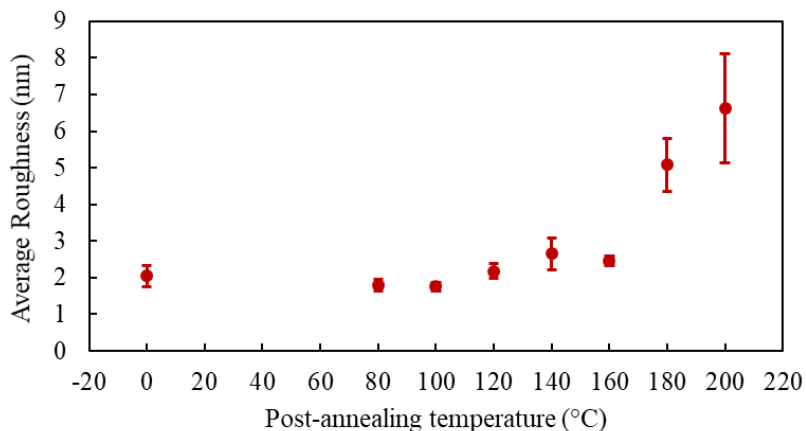


Figure 9. Organic Semiconductor (OSC) average roughness (RMS) versus post-annealing temperature. It shows an increasing trend.

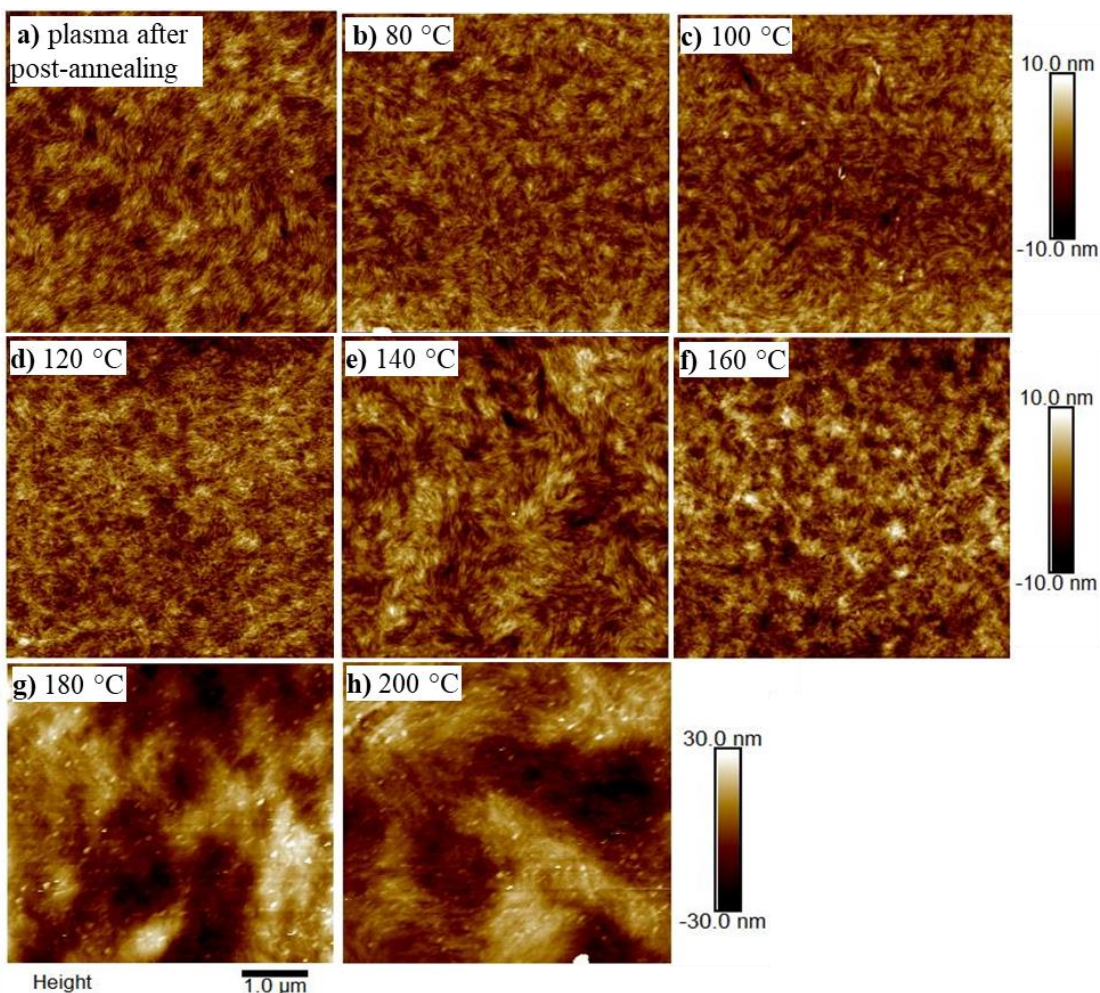


Figure 10. AFM images of the organic semiconductor on Teflon-AF (a) plasma treated after post-annealing (0 °C), post-annealed at (b) 80 °C, (c) 100 °C, (d) 120 °C, (e) 140 °C, (f) 160 °C, (g) 180 °C, and (h) 200 °C. Note that the scale of the scans is larger for 180 and 200 C due to the dewetting and large roughness of the OSC.

3.5 Bulk chemistry: FTIR Spectroscopy

To fully understand the scope of the change in the Teflon-AF films, FTIR spectroscopy using ATR was carried out on the samples. The spectra were studied to see whether the bulk of the material changed at all. The spectrum for the Teflon-AF solution is presented in Figure SI 4a. The main peaks at 1094 cm^{-1} , 1241 cm^{-1} , 1268 cm^{-1} , and 1305 cm^{-1} represent the fluorinated dioxole

group and the peak at 725 cm^{-1} shows the amorphous structure of the material [49,50]. Figure SI 4b-e show the spectra for Teflon-AF films before and after plasma-treatment, post-annealed at $120\text{ }^{\circ}\text{C}$ and $200\text{ }^{\circ}\text{C}$, respectively. These two specific temperatures represent samples post-annealed below and above T_g . The film spectra have the perfluoromethyl end-group $-\text{CF}_3$ peaks at 981 cm^{-1} , which does not appear in the solution spectrum [21,49]. This $-\text{CF}_3$ end-group has been reported to appear in the spectra for amorphous Teflon-AF powders and films that are not too thin [49]. The same peaks are observed in all of the film spectra, which suggests that no bulk modification has occurred. Previous FTIR characterization on Teflon-AF 1600 has also shown that it has good thermal stability below $400\text{ }^{\circ}\text{C}$ [51].

3.6 Surface chemistry: XPS measurements

Another explanation for the change in contact angle hysteresis after plasma treatment and after post-annealing could be changes in the surface chemistry of the Teflon-AF films. Here, we apply a similar approach to Teflon-AF using XPS to identify the chemical bonds that are intensified or weakened in each post-annealing step. The survey spectra include F 1s, O 1s, C 1s, and N 1s (weak) regions. Table 1 shows the change in the atomic percentage of the different elements. The total atomic percentages of fluorine atoms decreases after plasma treatment, but increases after post-annealing. Conversely, the atomic percentages of oxygen, carbon, and nitrogen atoms increase after air plasma treatment but decrease after post-annealing.

The core-level peaks in the C 1s region occur at the binding energies of 292 eV , 294.3 eV , 295.2 eV , 282 eV , 286.9 eV and 288.6 eV , which correspond to CF_2 [25,52,53], CF_3 [25,30,52–54], O-C-O [55], C-C [30,52] (or C-H [52,53]), C-O [30], and CF-CF [53] bonds respectively. The F 1s region of the spectra for the different conditions reveal the C-F [30] and $\text{CF}_2\text{-CF}_2$ [56] bonds for the core-level peaks at 689.1 eV and 691.1 eV , respectively. In the O 1s region, the peaks at 533.4 eV , 536.1 eV , 531.6 eV , and 537.3 eV represent C-O [30], O-CF_x [25], C-O-O [30], and O-C-O

[57,58] bonds respectively. Finally, the weak peak at 402.5 eV in the N 1s region indicates the appearance of C-N bonds [59] after plasma treatment. Figure 11a shows the survey spectrum for a sample post-annealed at 160 °C. The C 1s spectra for the different conditions are shown in Figure 11b with the two main peaks being distinguished with dashed lines. The changes in the concentration of the main bonds are plotted in Figure 11c. The percentage of fluorine-containing CF₂ (292 eV) and C-F (689.1 eV) bonds decreases after plasma treatment and increases again after post-annealing, while the percentage of oxygen-containing O-C-O (295.2 eV) and C-O (533.4 eV) bonds follows the opposite trend.

The change in the concentration of elements after plasma treatment and after post-annealing could be explained with two complementary scenarios. One, bonds containing oxygen and nitrogen form after plasma treatment. After post-annealing, these plasma-produced bonds dissociate, and fluorine-containing bonds reform [51]. Two, as has been suggested by Ref. [30], an overlayer containing air-plasma-produced oxygen and nitrogen atoms appears after plasma treatment, which covers the fluorinated surface of Teflon-AF, and reduces photoemission from the film underneath. Here, this overlayer is removed after the subsequent post-annealing step through a mechanism called surface adaptation. Surface adaptation, which is the continuous motion of the polymer chains from the surface to the bulk, has been observed in the ageing of PTFE films [20]. Both of these scenarios could explain the elemental percentage changes observed here. Bonds such as CF₂ (292 eV), show a higher percentage change from 16.8% to 10.2% after plasma treatment and back to 15.7% after post annealing, also O-C-O (295.2 eV), which changes from 1.8% to 7.7% and back to 3.7%. The change in some other bonds is smaller. For instance, C-F (689.1 eV) decreases from 55.6% to 54.7% after plasma treatment and increases back to 56% after post-annealing (Figure 11c). The shift in V_{th} with increasing post-annealing temperature (**Error! Reference source not found.b** and **Error! Reference source not found.e**) can be explained by the change in the oxygen content on the Teflon-AF surface. Oxygen plasma treatment shifts the threshold voltage to more positive values by introducing electron trapping sites at the interface [60,61]. Right after plasma treatment, V_{th} is -2 V, and it becomes more negative after post-annealing reaching -22 V at 200 °C. It is true that fluorine atoms have high electronegativity, and they can cause the trapping of electrons on the dielectric surface [16], but here we only see the effect of oxygen atoms.

We believe that the post-annealing step at elevated temperature resembles an accelerated ageing process where surface adaptation along with reformation of bonds at the surface cause the reversibility of films after post-annealing. The increase in advancing CA and decrease in CA hysteresis with post-annealing temperature shown in Figure 5a is therefore explained by the decrease in the percentage of reactive elements such as oxygen and the increase in the percentage of hydrophobic fluorine content on the surface. The lower percentage of reactive elements ensures a better OSC/dielectric interface with fewer trap sites, hence better OTFT performance. This also partly explains the improved OTFT performance for devices post-annealed below 180 °C, above which the OSC accumulates non-uniformly between the electrodes.

Table 1. Atomic percentages of oxygen, fluorine, carbon, and nitrogen before and after plasma and with annealing.

Atomic %					
	Before Plasma	After Plasma	80 °C	160 °C	200 °C
O 1s	10.6	11.9	11.6	10.7	10.8
F 1s	58.0	55.6	55.8	57.5	57.6
C 1s	31.4	32.5	32.6	31.7	31.5
N 1s	0.0	0.4	0.3	0.1	0.0

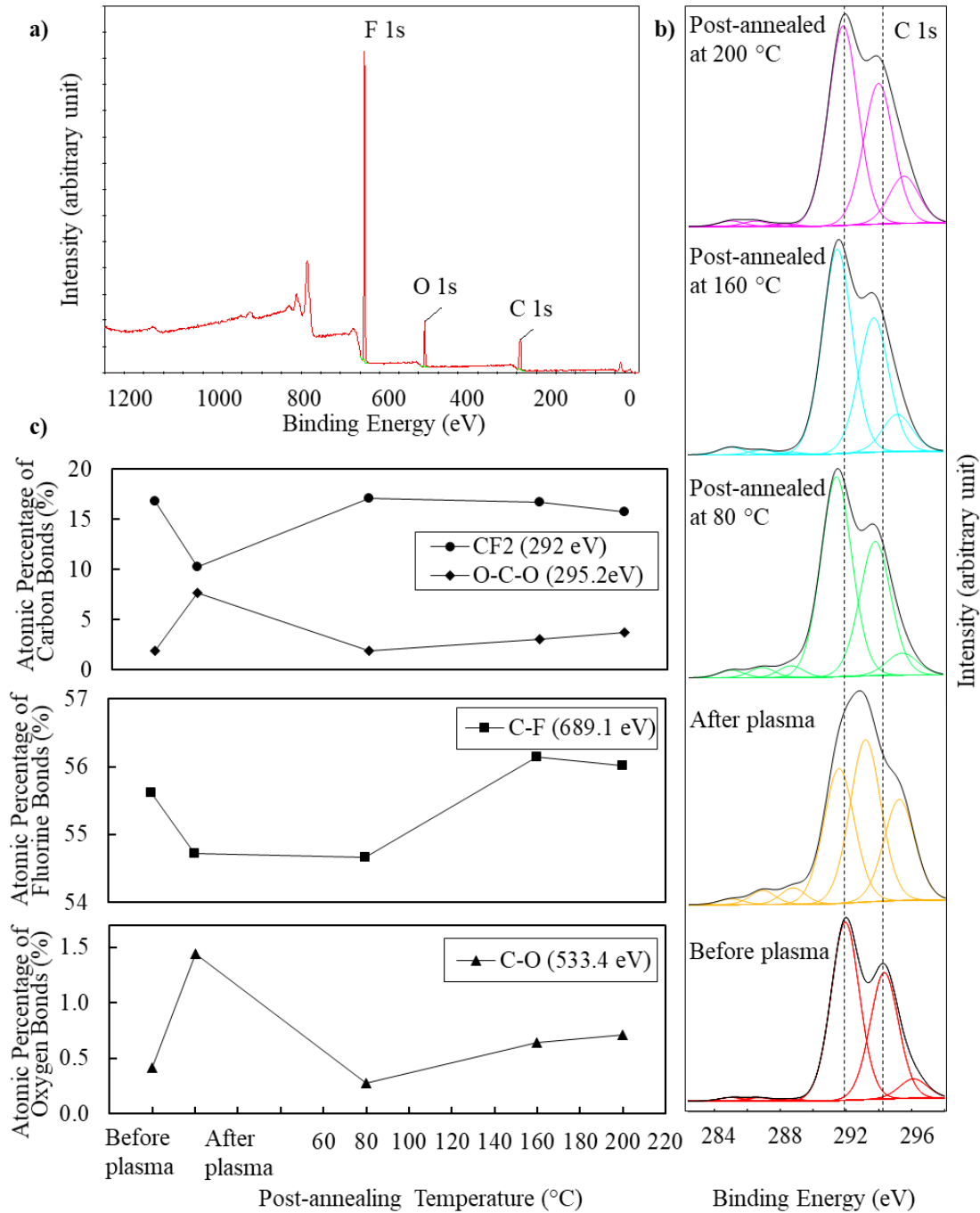


Figure 11. (a) XPS survey spectrum for Teflon-AF post-annealed at 160 °C, (b) C 1s spectra for different conditions, with the dashed lines specifying the two main peaks at 292 eV and 294.3 eV, and (c) the change in the percentages of the CF₂, O-C-C, C-F, and C-O bonds.

4. Conclusions

OTFTs with inkjet-printed electrodes on hydrophobic fluoropolymer gate dielectric were fabricated. Plasma treatment was used to increase the wettability of the fluoropolymer. However, printing and annealing of the electrodes add complications to the gate dielectric/ OSC interface that have not been studied before. We show that surface reversibility of Teflon-AF changes the morphological and chemical properties on the surface after plasma treatment and after subsequent post-annealing at different temperatures. The contact angle hysteresis and surface roughness increase and reactive elements appear on the surface after plasma treatment. However, after post-annealing, the opposite trend is observed. The reactive elements disappear and the random roughness on the surface changes to ordered grain-like structures with increasing post-annealing temperature from 80 °C to 140 °C. At 160 °C, the surface starts smoothing and at 200 °C it changes back to the state before plasma treatment. Hence, at the right temperature, the desired wettability, roughness, and percentage of chemical bonds can be achieved. At this temperature (160 °C), OTFT parameters such as field-effect mobility and on-off current ratio are maximized. To prove that the OSC/ dielectric interface is the dominant effect rather than contact resistance, we extracted the contact resistance and low-field mobility. The low-field mobility that is independent of contact resistance shows a clear trend with post-annealing temperature. Low-field mobility is increased by a factor of approximately five from 80 °C to 160 °C post-annealing temperature, leading to improved transistor performance. This study of Teflon-AF enables control over the OSC/ dielectric interfacial properties in printed OTFTs for improved device performance as well as surface engineering in many other applications of fluoropolymers.

Acknowledgements

We acknowledge the support of the Natural Sciences and Engineering Research Council of Canada (NSERC), funding reference number STPGP 521480-18. AFM images and FTIR spectra were taken at the Mechanical Engineering department at York University. We thank Dr. Thomas Cooper for giving us access to his FTIR spectrometer. XPS results were taken at the Ontario Centre for the Characterization of Advanced Materials (OCCAM) at the University of Toronto.

References

- [1] Y. Bonnassieux, C.J. Brabec, Y. Cao, T.B. Carmichael, M.L. Chabiny, K.T. Cheng, G. Cho, A. Chung, C.L. Cobb, A. Distler, H.J. Egelhaaf, G. Grau, X. Guo, G. Haghighashtiani, T.C. Huang, M.M. Hussain, B. Iniguez, T.M. Lee, L. Li, Y. Ma, D. Ma, M.C. McAlpine, T.N. Ng, R. Österbacka, S.N. Patel, J. Peng, H. Peng, J. Rivnay, L. Shao, D. Steingart, R.A. Street, V. Subramanian, L. Torsi, Y. Wu, The 2021 flexible and printed electronics roadmap, *Flex. Print. Electron.* 6 (2021) 023001. <https://doi.org/10.1088/2058-8585/ABF986>.
- [2] J.W. Borchert, J.W. Borchert, U. Zschieschang, F. Letzkus, M. Giorgio, M. Giorgio, R.T. Weitz, R.T. Weitz, R.T. Weitz, M. Caironi, J.N. Burghartz, S. Ludwigs, H. Klauk, Flexible low-voltage high-frequency organic thin-film transistors, *Sci. Adv.* 6 (2020). https://doi.org/10.1126/SCIADV.AAZ5156/SUPPL_FILE/AAZ5156_SM.PDF.
- [3] G. Grau, R. Kitsomboonloha, S.L. Swisher, H. Kang, V. Subramanian, Printed transistors on paper: Towards smart consumer product packaging, *Adv. Funct. Mater.* 24 (2014) 5067–5074. <https://doi.org/10.1002/adfm.201400129>.
- [4] G. Grau, V. Subramanian, Dimensional scaling of high-speed printed organic transistors enabling high-frequency operation, *Flex. Print. Electron.* 5 (2020) 014013. <https://doi.org/10.1088/2058-8585/AB739A>.
- [5] A. Salleo, Charge transport in polymeric transistors, *Mater. Today.* 10 (2007) 38–45. [https://doi.org/10.1016/S1369-7021\(07\)70018-4](https://doi.org/10.1016/S1369-7021(07)70018-4).

- [6] A. Facchetti, M.-H. Yoon, T.J. Marks, Gate Dielectrics for Organic Field-Effect Transistors: New Opportunities for Organic Electronics, *Adv. Mater.* 17 (2005) 1705–1725. <https://doi.org/10.1002/ADMA.200500517>.
- [7] F. Dinelli, M. Murgia, P. Levy, M. Cavallini, F. Biscarini, D.M. de Leeuw, Spatially Correlated Charge Transport in Organic Thin Film Transistors, *Phys. Rev. Lett.* 92 (2004) 116802. <https://doi.org/10.1103/PhysRevLett.92.116802>.
- [8] W.C. Shin, S. Seo, B.J. Cho, Highly air-stable electrical performance of graphene field effect transistors by interface engineering with amorphous fluoropolymer, *Appl. Phys. Lett.* 98 (2011) 153505. <https://doi.org/10.1063/1.3578396>.
- [9] J. Lefebvre, J. Ding, Z. Li, F. Cheng, N. Du, P.R.L. Malenfant, Hysteresis free carbon nanotube thin film transistors comprising hydrophobic dielectrics, *Appl. Phys. Lett.* (2015). <https://doi.org/10.1063/1.4937223>.
- [10] Y. Jung, R. Joseph Kline, D.A. Fischer, R.J. Kline, M. Heeney, L. McCulloch, D.M. DeLongchamp, The Effect of Interfacial Roughness on the Thin Film Morphology and Charge Transport of High-Performance Polythiophenes, *Adv. Funct. Mater.* 18 (2008) 742–750. <https://doi.org/10.1002/ADFM.200701089>.
- [11] K.P. Pernstich, D. Oberhoff, C. Goldmann, B. Batlogg, Modeling the water related trap state created in pentacene transistors, *Appl. Phys. Lett.* 89 (2006) 213509. <https://doi.org/10.1063/1.2396924>.
- [12] S.H. Lee, Y. Xu, D. Khim, W.T. Park, D.Y. Kim, Y.Y. Noh, Effect of Polymer Gate Dielectrics on Charge Transport in Carbon Nanotube Network Transistors: Low-k Insulator for Favorable Active Interface, *ACS Appl. Mater. Interfaces.* 8 (2016) 32421–32431. https://doi.org/10.1021/ACSAMI.6B06882/SUPPL_FILE/AM6B06882_SI_001.PDF.
- [13] S. Ebnesajjad, *Introduction to Fluoropolymers: Materials, Technology, and Applications*, 2020.
- [14] B. Ameduri, Fluoropolymers: The Right Material for the Right Applications, *Chem. – A Eur. J.* 24 (2018) 18830–18841. <https://doi.org/10.1002/CHEM.201802708>.

- [15] F. He, K. Jin, J. Wang, Y. Luo, J. Sun, Q. Fang, F. He, K. Jin, J. Wang, Y. Luo, J. Sun, Q. Fang, New Fluoropolymers Having Both Low Water Uptake and a Low Dielectric Constant, *Macromol. Chem. Phys.* 216 (2015) 2302–2308.
<https://doi.org/10.1002/MACP.201500394>.
- [16] K.J. Baeg, Y.Y. Noh, D.Y. Kim, Charge transfer and trapping properties in polymer gate dielectrics for non-volatile organic field-effect transistor memory applications, *Solid. State. Electron.* 53 (2009) 1165–1168. <https://doi.org/10.1016/J.SSE.2009.07.003>.
- [17] T. Sekine, H. Ikeda, A. Kosakai, K. Fukuda, D. Kumaki, S. Tokito, Improvement of mechanical durability on organic TFT with printed electrodes prepared from nanoparticle ink, *Appl. Surf. Sci.* (2014). <https://doi.org/10.1016/j.apsusc.2013.12.168>.
- [18] K. Fukuda, Y. Takeda, Y. Kobayashi, M. Shimizu, T. Sekine, D. Kumaki, M. Kurihara, M. Sakamoto, S. Tokito, Patterning method for silver nanoparticle electrodes in fully solution-processed organic thin-film transistors using selectively treated hydrophilic and hydrophobic surfaces, *Jpn. J. Appl. Phys.* (2013).
<https://doi.org/10.7567/JJAP.52.05DB05>.
- [19] A. Pierre, M. Sadeghi, M.M. Payne, A. Facchetti, J.E. Anthony, A.C. Arias, All-printed flexible organic transistors enabled by surface tension-guided blade coating, *Adv. Mater.* (2014). <https://doi.org/10.1002/adma.201401520>.
- [20] S. Zanini, R. Barni, R. Della Pergola, C. Riccardi, Modification of the PTFE wettability by oxygen plasma treatments: influence of the operating parameters and investigation of the ageing behaviour, *J. Phys. D. Appl. Phys.* 47 (2014) 325202.
<https://doi.org/10.1088/0022-3727/47/32/325202>.
- [21] N. Sprang, D. Theirich, J. Engemann, Surface modification of fluoropolymers by microwave plasmas: FTIR investigations, *Surf. Coatings Technol.* 98 (1998) 865–871.
[https://doi.org/10.1016/S0257-8972\(97\)00362-9](https://doi.org/10.1016/S0257-8972(97)00362-9).
- [22] D.J. Wilson, R.L. Williams, R.C. Pond, Plasma modification of PTFE surfaces - Part I: Surfaces immediately following plasma treatment, *Surf. Interface Anal.* 31 (2001) 385–396. <https://doi.org/10.1002/SIA.1065/FORMAT/PDF>.

- [23] A. Vesel, M. Mozetic, A. Zalar, XPS characterization of PTFE after treatment with RF oxygen and nitrogen plasma, *Surf. Interface Anal.* 40 (2008) 661–663. <https://doi.org/10.1002/SIA.2691>.
- [24] N. Vandencastele, D. Merche, F. Reniers, XPS and contact angle study of N₂ and O₂ plasma-modified PTFE, PVDF and PVF surfaces, *Surf. Interface Anal.* 38 (2006) 526–530. <https://doi.org/10.1002/SIA.2255>.
- [25] C.-C. Cho, R.M. Wallace, L.A. Files-Sesler, Patterning and Etching of Amorphous Teflon Films, *J. Electron. Mater.* 23 (1994).
- [26] W.L. Kalb, T. Mathis, S. Haas, A.F. Stassen, B. Batlogg, Organic small molecule field-effect transistors with Cytop™ gate dielectric: Eliminating gate bias stress effects, *Appl. Phys. Lett.* 90 (2007) 092104. <https://doi.org/10.1063/1.2709894>.
- [27] B. Sun, W. Hong, Z. Yan, H. Aziz, Y. Li, Record High Electron Mobility of 6.3 cm² V⁻¹ s⁻¹ Achieved for Polymer Semiconductors Using a New Building Block, *Adv. Mater.* 26 (2014) 2636–2642. <https://doi.org/10.1002/adma.201305981>.
- [28] G. Kitahara, K. Aoshima, J. Tsutsumi, H. Minemawari, S. Arai, T. Hasegawa, Low-voltage operation of organic thin-film transistors based on ultrafine printed silver electrodes, *Org. Electron.* 50 (2017) 426–428. <https://doi.org/10.1016/J.ORGEL.2017.08.023>.
- [29] M. Trapuzzano, N.B. Crane, R. Guldiken, A. Tejada-Martínez, Wetting metamorphosis of hydrophobic fluoropolymer coatings submerged in water and ultrasonically vibrated, *J. Coatings Technol. Res.* 2019 173. 17 (2019) 633–642. <https://doi.org/10.1007/S11998-019-00250-1>.
- [30] A.K. Gnanappa, C. O'Murchu, O. Slattery, F. Peters, B. Aszalós-Kiss, S.A.M. Tofail, Effect of annealing on hydrophobic stability of plasma deposited fluoropolymer coatings, *Polym. Degrad. Stab.* 93 (2008) 2119–2126. <https://doi.org/10.1016/J.POLYMDEGRADSTAB.2008.08.012>.
- [31] Y.-C. Lo, D. Li, Z. Sun, S. Shaik, X. Cheng, High-resolution nondestructive patterning of isolated organic semiconductors, *J. Vac. Sci. Technol. B, Nanotechnol. Microelectron.*

- Mater. Process. Meas. Phenom. (2012). <https://doi.org/10.1116/1.4757956>.
- [32] S. Wang, X. Zhao, Y. Tong, Q. Tang, Y. Liu, S. Wang, X. Zhao, Y. Tong, Q. Tang, Y. Liu, Directly Spin Coating a Low-Viscosity Organic Semiconductor Solution onto Hydrophobic Surfaces: Toward High-Performance Solution-Processable Organic Transistors, *Adv. Mater. Interfaces*. 7 (2020) 1901950. <https://doi.org/10.1002/ADMI.201901950>.
- [33] B.J. Kang, J.H. Oh, Control of the crystalline structure of inkjet-printed semiconductor layers using overlap condition and surface wettability, *J. Micromechanics Microengineering*. 25 (2015) 055011. <https://doi.org/10.1088/0960-1317/25/5/055011>.
- [34] B. Sun, W. Hong, H. Aziz, Y. Li, A pyridine-flanked diketopyrrolopyrrole (DPP)-based donor–acceptor polymer showing high mobility in ambipolar and n-channel organic thin film transistors, *Polym. Chem*. 6 (2015) 938–945. <https://doi.org/10.1039/C4PY01193G>.
- [35] Q. Liu, Y. Wang, A. Kohara, H. Matsumoto, S. Manzhos, K. Feron, S.E. Bottle, J. Bell, T. Michinobu, P. Sonar, Tuning the Charge Carrier Polarity of Organic Transistors by Varying the Electron Affinity of the Flanked Units in Diketopyrrolopyrrole-Based Copolymers, *Adv. Funct. Mater*. 30 (2020) 1907452. <https://doi.org/10.1002/ADFM.201907452>.
- [36] O.D. Jurchescu, M. Popinciuc, B.J. Van Wees, T.T.M. Palstra, Interface-controlled, high-mobility organic transistors, *Adv. Mater*. 19 (2007) 688–692. <https://doi.org/10.1002/ADMA.200600929/FORMAT/PDF>.
- [37] J. Dong, P. Yu, S.A. Arabi, J. Wang, J. He, C. Jiang, Enhanced mobility in organic field-effect transistors due to semiconductor/dielectric interface control and very thin single crystal, *Nanotechnology*. 27 (2016) 275202. <https://doi.org/10.1088/0957-4484/27/27/275202>.
- [38] Y. Xu, T. Minari, K. Tsukagoshi, J.A. Chroboczek, G. Ghibaudo, Direct evaluation of low-field mobility and access resistance in pentacene field-effect transistors, *J. Appl. Phys*. 107 (2010) 114507. <https://doi.org/10.1063/1.3432716>.
- [39] Shichao Zhang, Yunfeng Qiu, Huihui Yang, Dao Wang, Yunxia Hu, Xubing Lu,

- Zhonghua Li, PingAn Hu, The role of hybrid dielectric interfaces in improving the performance of multilayer InSe transistors, *J. Mater. Chem. C.* 8 (2020) 6701–6709. <https://doi.org/10.1039/D0TC00331J>.
- [40] T.S. Meiron, A. Marmur, I.S. Saguy, Contact angle measurement on rough surfaces, *J. Colloid Interface Sci.* 274 (2004) 637–644. <https://doi.org/10.1016/J.JCIS.2004.02.036>.
- [41] J.D. Miller, S. Veeramasuneni, J. Drelich, M.R. Yalamanchili, G. Yamauchi, Effect of roughness as determined by atomic force microscopy on the wetting properties of PTFE thin films, *Polym. Eng. Sci.* 36 (1996) 1849–1855. <https://doi.org/10.1002/PEN.10580>.
- [42] Q. Liu, J. Yu, H. Wang, The role of the substrate roughness in contact angle hysteresis and dynamic deviation, *Int. J. Heat Mass Transf.* 148 (2020) 118985. <https://doi.org/10.1016/J.IJHEATMASSTRANSFER.2019.118985>.
- [43] Y. Li, C. Liu, Y. Xu, T. Minari, P. Darmawan, K. Tsukagoshi, Solution-processed organic crystals for field-effect transistor arrays with smooth semiconductor/dielectric interface on paper substrates, *Org. Electron.* 13 (2012) 815–819. <https://doi.org/10.1016/J.ORGEL.2012.01.021>.
- [44] G. Horowitz, M.E. Hajlaoui, Grain size dependent mobility in polycrystalline organic field-effect transistors, *Synth. Met.* 122 (2001) 185–189. [https://doi.org/10.1016/S0379-6779\(00\)01351-5](https://doi.org/10.1016/S0379-6779(00)01351-5).
- [45] M. Geiger, R. Acharya, E. Reutter, T. Ferschke, U. Zschieschang, J. Weis, J. Pflaum, H. Klauk, R.T. Weitz, Effect of the Degree of the Gate-Dielectric Surface Roughness on the Performance of Bottom-Gate Organic Thin-Film Transistors, *Adv. Mater. Interfaces.* 7 (2020) 1902145. <https://doi.org/10.1002/ADMI.201902145>.
- [46] J. Wang, Y. Wu, Y. Cao, G. Li, Y. Liao, Influence of surface roughness on contact angle hysteresis and spreading work, (n.d.). <https://doi.org/10.1007/s00396-020-04680-x/Published>.
- [47] D.M. Spori, T. Drobek, S. Zürcher, M. Ochsner, C. Sprecher, A. Mühlebach, N.D. Spencer, Beyond the Lotus Effect: Roughness Influences on Wetting over a Wide Surface-Energy Range, *Langmuir.* 24 (2008) 5411–5417.

<https://doi.org/10.1021/LA800215R>.

- [48] G. Bracco, B. Holst, *Surface Science Techniques*, Springer Science & Business Media, 2013.
- [49] T.C. Nason, J.A. Moore, T. -M. Lu, Deposition of amorphous fluoropolymer thin films by thermolysis of Teflon amorphous fluoropolymer, *Appl. Phys. Lett.* 60 (1998) 1866. <https://doi.org/10.1063/1.107163>.
- [50] M. Abdmouleh, I. Jedidi, M. Khitouni, A. Ben Salah, A. Kabadou, LDPE PHASE COMPOSITION IN LDPE/Cu COMPOSITES USING THERMAL ANALYSIS AND FTIR SPECTROSCOPY, (n.d.).
- [51] S.J. Ding, P.F. Wang, X.G. Wan, D.W. Zhang, J.T. Wang, W.W. Lee, Effects of thermal treatment on porous amorphous fluoropolymer film with a low dielectric constant, *Mater. Sci. Eng. B.* 83 (2001) 130–136. [https://doi.org/10.1016/S0921-5107\(01\)00504-9](https://doi.org/10.1016/S0921-5107(01)00504-9).
- [52] N. Cioffi, L. Torsi, I. Farella, D. Altamura, A. Valentini, N. Ditaranto, L. Sabbatini, P.G. Zambonin, T. Bleve-Zacheo, Deposition and analytical characterization of fluoropolymer thin films modified by palladium nanoparticles, *Thin Solid Films.* 449 (2004) 25–33. <https://doi.org/10.1016/J.TSF.2003.10.016>.
- [53] L. Sandrin, M.S. Silverstein, E. Sacher, Fluorine incorporation in plasma-polymerized octofluorocyclobutane, hexafluoropropylene and trifluoroethylene, *Polymer (Guildf).* 42 (2001) 3761–3769. [https://doi.org/10.1016/S0032-3861\(00\)00693-5](https://doi.org/10.1016/S0032-3861(00)00693-5).
- [54] Y. Suzuki, H. Fu, Y. Abe, M. Kawamura, Effects of substrate temperature on structure and mechanical properties of sputter deposited fluorocarbon thin films, *Vacuum.* 87 (2013) 218–221. <https://doi.org/10.1016/J.VACUUM.2012.05.029>.
- [55] J. Gardella, S.A. Ferguson, R.L. Chin, $\pi^* \leftarrow \pi$ Shakeup Satellites for the Analysis of Structure and Bonding in Aromatic Polymers by X-Ray Photoelectron Spectroscopy:, <Http://Dx.Doi.Org/10.1366/0003702864509565>. 40 (2016) 224–232. <https://doi.org/10.1366/0003702864509565>.
- [56] J.A. Taylor, G.M. Lancaster, J.W. Rabalais, Surface alteration of graphite, graphite monofluoride and teflon by interaction with Ar⁺ and Xe⁺ beams, *Appl. Surf. Sci.* 1 (1978)

- 503–514. [https://doi.org/10.1016/0378-5963\(78\)90027-2](https://doi.org/10.1016/0378-5963(78)90027-2).
- [57] T.G. Avval, S. Chatterjee, S. Bahr, P. Dietrich, M. Meyer, A. Thißen, M.R. Linford, Carbon dioxide gas, CO₂(g), by near-ambient pressure XPS, *Surf. Sci. Spectra*. 26 (2019) 014022. <https://doi.org/10.1116/1.5053761>.
- [58] G. De La Puente, J.J. Pis, J.A. Menéndez, P. Grange, Thermal stability of oxygenated functions in activated carbons, *J. Anal. Appl. Pyrolysis*. 43 (1997) 125–138. [https://doi.org/10.1016/S0165-2370\(97\)00060-0](https://doi.org/10.1016/S0165-2370(97)00060-0).
- [59] D.S. Everhart, C.N. Reilley, Polymer functional group mobility. 2—Partition of ion pairs between hydrophobic and hydrophilic phases of plasma oxidized polyethylene, *Surf. Interface Anal.* 3 (1981) 258–268. <https://doi.org/10.1002/SIA.740030606>.
- [60] Y. Qiu, P. Wei, Z. Wang, W. Lu, Y. Jiang, C. Zhang, Y. Qu, G. Lu, Manipulating Doping of Organic Semiconductors by Reactive Oxygen for Field-Effect Transistors, *Phys. Status Solidi – Rapid Res. Lett.* 12 (2018) 1800297. <https://doi.org/10.1002/PSSR.201800297>.
- [61] Y. Kimura, M. Kitamura, A. Kitani, Y. Arakawa, Operational stability in pentacene thin-film transistors with threshold voltages tuned by oxygen plasma treatment, *Jpn. J. Appl. Phys.* 55 (2016) 02BB14. <https://doi.org/10.7567/JJAP.55.02BB14/XML>.